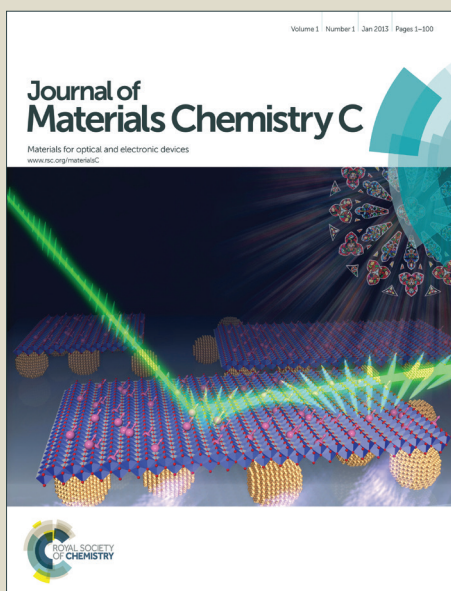


Journal of Materials Chemistry C

Accepted Manuscript



This is an *Accepted Manuscript*, which has been through the Royal Society of Chemistry peer review process and has been accepted for publication.

Accepted Manuscripts are published online shortly after acceptance, before technical editing, formatting and proof reading. Using this free service, authors can make their results available to the community, in citable form, before we publish the edited article. We will replace this *Accepted Manuscript* with the edited and formatted *Advance Article* as soon as it is available.

You can find more information about *Accepted Manuscripts* in the [Information for Authors](#).

Please note that technical editing may introduce minor changes to the text and/or graphics, which may alter content. The journal's standard [Terms & Conditions](#) and the [Ethical guidelines](#) still apply. In no event shall the Royal Society of Chemistry be held responsible for any errors or omissions in this *Accepted Manuscript* or any consequences arising from the use of any information it contains.

Cite this: DOI: 10.1039/c0xx00000x

ARTICLE TYPE

www.rsc.org/xxxxxx

Large area uniformly oriented multilayer graphene with high transparent and conducting properties derived from highly oriented polyethylene film

Bing He^a, Zhongjie Ren^a, Shouke Yan^{*a} and Zhaohui Wang^{*b}*Received (in XXX, XXX) Xth XXXXXXXXX 20XX, Accepted Xth XXXXXXXXX 20XX*

DOI: 10.1039/b000000x

In this study, well-ordered multilayer graphene have been obtained via highly oriented polyethylene (OPE) film. Optical microscopy (OM), atomic force microscopy (AFM), Raman laser spectroscopy, scanning electron microscopy (SEM) and transmission electron microscopy (TEM) results indicated that the obtained graphene films were continuous and uniform in lattice orientation. Optical and electrical characterization of the prepared graphene revealed that the thin films are stable in air conditions and exhibit higher optical and electrical properties than that obtained from non-oriented polyethylene (nOPE).

1. Introduction

Graphene is the most promising potential successor to silicon for fabricating next-generation electronic devices at present owing to its fascinating physical properties.¹ Since the discovery of the first isolated graphene prepared by mechanical exfoliation of graphite crystals, many chemical approaches for synthesizing large-scale graphene have been developed, including chemical vapor deposition (CVD),^{2, 3} epitaxial growth on silicon carbide,⁴⁻⁶ thermal or chemical reduction of graphite oxide (GO),⁷⁻¹¹ and bottom-up organic synthesis.¹²⁻¹⁴ Plenty of researches have been focused on developing route for obtaining large area of monolayer, bilayer or multilayer graphene by CVD of CH₄ or C₂H₂ gases on metal substrates.¹⁵⁻¹⁷ However, CVD is limited to the use of gaseous raw materials, making it difficult to apply the technology to a wider variety of potential feedstocks. Moreover, the continuity and uniformity of graphene film obtained with CVD method is hardly controllable. In view of these, large area continuous graphene with controllable thickness has been grown from different solid carbon sources, such as polymer films or small molecules.¹⁸⁻²¹

It is reported that graphene is optically highly transparent which makes it a candidate for a high quality transparent conductive electrode.²²⁻²⁵ Currently, graphene is applied in many frontiers such as supercapacitor,²⁶⁻³⁰ solar cell electrodes,³¹ lithium ion battery anodes,³² and optoelectronic applications.^{33, 34} For this purpose, uniform microstructure of graphene is very important. Therefore, self-organization into graphene lattice from atoms or molecules is interesting as it permits the potential manipulation of graphene morphology (related to internal crystalline structures)

for tuning its electrical and optical properties by controlling the related conditions.³⁵ However, large area of graphene film with uniform interlamellar structure cannot be easily obtained by the previous methods mentioned above, including CVD. Thus, a controllable synthesis technique is highly desirable to grow uniform and regular interlamellar structure of multilayer graphene.

Here, we report a new method of growing well-ordered multilayer graphene membrane derived from solid carbon source. In this process, highly oriented polyethylene (OPE) films with well arranged lamellar structure were obtained by a melt-draw technique.³⁶⁻³⁸ With rapid heating of the prepared OPE films to 1000 °C, the oriented carbon chains transform into carbon rings immediately without the process of melt and disorientation. One of the major benefits of our method is that the multilayer graphene grows in same way and has a fine lattice matching between the adjacent layers, which produce a large area, continuous and homogeneous multilayer graphene with regular lattice structure. This is hardly achieved by many other methods.^{2, 39-43} Meanwhile, the optical and electrical properties of the obtained graphene films, which are quite stable in air condition, are higher than those produced by many other methods.

2. Experimental Details

2.1 Preparation of OPE and nOPE film

Highly oriented PE ultra-thin films were prepared according to a melt-draw technique. According to this method, as schematically presented in the left part of Scheme 1, a small amount of a 0.3 ~ 1 wt% PE solution

in xylene was poured and uniformly spread on a preheated glass plate at a temperature within a window from 122 °C to 130 °C, at which the solvent was allowed to evaporate. In order to avoid temperature fluctuations, the heating plate was placed in a specially prepared small cabinet. After evaporating the solvent, the remaining molten polymer film of thickness ~0.5 μm was picked up by a motor-driven cylinder with a drawing speed of ~20cm/s. The resultant PE ultrathin films of 30 to 50 nm in thickness are highly oriented as tested by transmission electron microscopy (TEM) observation. Bright field electron micrograph shows that the thus prepared OPE film exhibit well ordered lamellar structure (see Figure S1a). Electron diffraction of the melt-drawn PE highly oriented thin films confirms the high orientation of them with molecular chains in film plane and along the drawing direction (see the electron diffraction pattern shown in Fig. S1b).

To get nOPE films, the melt-drawn OPE films were annealed at 140 °C for 5 min. After the heat-treatment, the PE molecular chains rearranged randomly. Copper foil of 25-μm-thick (Alfa Aesar, 99.98%) was used as the substrate. Both the OPE and nOPE films were adhered to the surface of copper substrates for the subsequent experiments.

2.2 Growth of multilayer graphene on copper substrates.

A typical process was used as follows. A standard 1-inch quartz tube in a furnace was evacuated to ~50 mTorr using a vacuum pump. Then, H₂ and Ar gases were fed into the apparatus, maintaining the total pressure at atmospheric pressure. The temperature was maintained at 1000 °C. Sample placed in a quartz boat was moved to the hot region at 1000 °C using a magnetic rod and annealed at this temperature for 15 min. It was subsequently fast-cooled by quickly removing it from the hot-zone of the furnace to room temperature using the magnetic rod. Rapid heating and cooling of the sample are essential. It is useful to be able to control the thickness by tuning the growth parameters when producing the graphene.²¹ One sample (OGP1) was produced from the as-made OPE films with the flow rates of Ar and H₂ gases of 500 sccm and 50 sccm, respectively. Another sample (OGP2) was produced from the as-made OPE films but with Ar and H₂ flow rates of 500 sccm and 10 sccm, respectively. For direction comparison, samples derived from nOPE, referred as nOGP is produced same as the OGP1.

2.3 Copper film etching and transferring process.

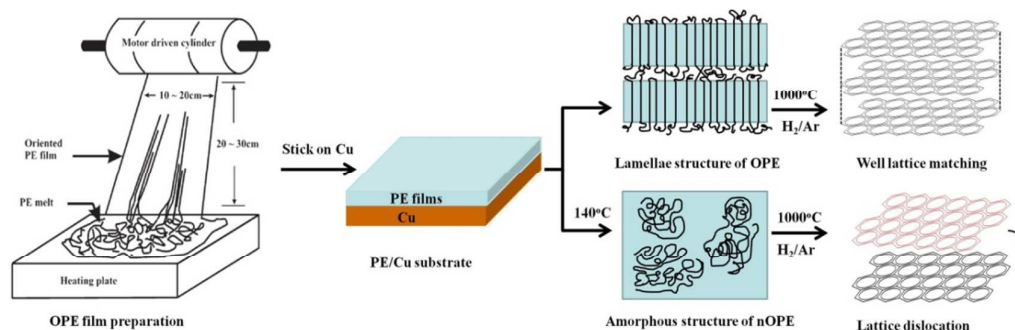
The graphene grown on copper foil was transferred onto Si substrate with 300 nm layer silicon-dioxide (SiO₂), quartz substrate after ultrasonic cleaning in trichloromethane solution and TEM grid by polymer-assisted method through etching the copper foils in Marble's reagent similar to previous reported methods.²¹ Briefly, before placing Graphene/Cu in the Marble's reagent, the surface of the copper covered with thin graphene layer was first coated with poly (methymethacrylate) (PMMA) and then dried in an oven at 120 °C for 5 min. After the complete removal of the copper foil, the PMMA/Graphene film was rinsed with deionized water for several times to remove the residual Marble's reagent and then the PMMA/Graphene film was attached to other substrates as mentioned above followed by dried in an oven at 100 °C for 15 min. After this, the PMMA was removed by hot acetone solution.

2.4 Device fabrication and performance measurements.

Devices were fabricated on SiO₂/Si wafer for electrical conductivity measurements and quartz wafer for transmittance and sheet resistance measurements with Au as electrodes. Au electrodes were fabricated onto the graphene film by evaporation through a shadow mask. The Au electrodes fabricated in this study have a total thickness of 50 nm. The sheet resistance was measured using four-probe method in air at different temperature. More details of the characterization are described in the supporting information.

3. Result and Discussion

Scheme 1 presents the preparation processes of graphene from OPE and nOPE thin films. The self-assembly of oriented and disoriented PE molecular chains into multilayer graphene structure involves the hexatomic ring formation and dehydrogenation on Cu surface under 1000 °C. The building blocks are energetically active to organize themselves into ordered structures by surface diffusion, being similar to the process of common CVD process involving C atoms.²⁰ Because of the ordered arrangement of PE molecular chains, low energy may be needed in the formation of graphene interlayers. The formation mechanism of the adjacent graphene layer follows the regular structure of PE lamellae. In contrast, the PE molecular chains in OPE films after annealing at 140 °C are disoriented. The formation mechanism of the adjacent graphene layer obeys the lowest energy principle thus result in a lattice displacement between the neighbour layers.



Scheme 1 Schematic of OGP and nOGP grown on a copper surface where the black lines represent PE molecular chains.

The OGP1 film was transferred onto silicon wafers with an oxide layer of 300 nm for optical microscopy (OM) observation. As shown in Fig. 1a, the large area in light blue corresponds to the as-made graphene membrane, while the cracks in dark blue is associated to the silicon substrate, which were slashed intentionally for the thickness measurement of the graphene membrane by atomic force microscopy (AFM). The black particles are inevitable impurities introduced during annealing or transfer processes. The OM observation shows that the obtained graphene is a large area, continuous and homogeneous membrane with few defects.

AFM was used to probe the fine morphology and thickness of graphene membranes afterwards. Fig. 1b and Fig. 2a are the AFM images of different thickness graphene on the silicon substrates obtained from OPE films. As seen from the height analysis, the OGP1 membrane is ~ 4.8 nm, which is the corresponding areas marked with number "1" in Fig. 1a, while OGP2 is ~ 15.6 nm. Both of the AFM height analyses images taken at the different areas of OGP1 surface show similar thickness and microstructures which can be seen in Fig. 1b and Fig. S2 in the supporting information, indicating that OGP1 film is continuous and homogeneous. As shown in Fig. 2b, the thickness of nOGP is ~ 5 nm which is similar to OGP1. However, the surface of nOGP is rougher than that of OGP1, which can be observed from the height analysis. The AFM images also show wrinkled and rippled structures on the graphene surface which are most likely caused by Cu contraction due to the different thermal expansion coefficients of graphene and copper substrate during cooling process, which is consistent with the observation previous reported.⁴⁴ In addition, the white substance left on the surface of graphene is

the residual PMMA resulting from the transfer process from metals.⁴⁵

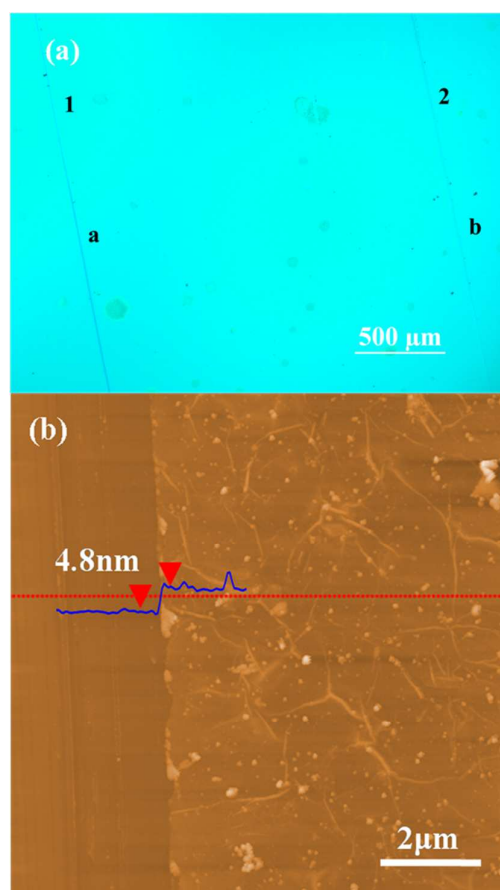


Fig. 1 (a) Optical image of OGP1, (b) AFM analysis of OGP1 corresponding to the location denoted with number "1" in Fig. 1a.

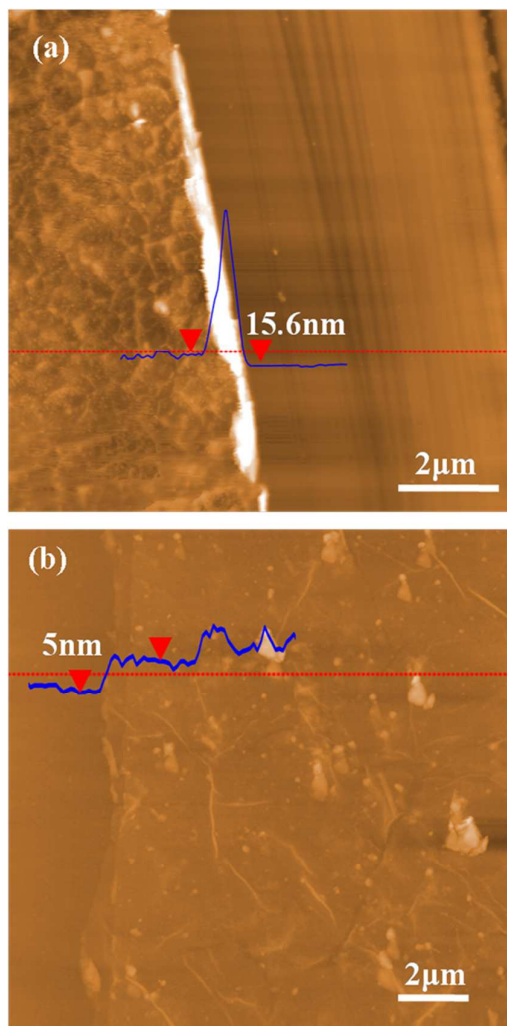


Fig. 2 AFM images of (a) OGP2 and (b) nONGP films on the SiO_2/Si substrate.

Raman spectroscopy is a powerful tool for identifying graphene. The Raman spectra of OGP1 and nONGP are shown in Fig. 3a-c, respectively. The major features of the Raman spectra of graphene are the G band locating at around $1560\text{--}1600\text{ cm}^{-1}$ and the 2D band at $\sim 2700\text{ cm}^{-1}$.⁴⁶ The G band is the result of first-order scattering of the E_{2g} mode observed for sp^2 carbon domains, and the 2D band is the most prominent feature in the Raman spectra of high-quality graphene.⁴⁷ The D band at $1335\text{--}1350\text{ cm}^{-1}$ usually indicates the presence of few sp^3 carbon atoms or defects.⁴⁸ The intensity ratio of D-band and G-band (I_D/I_G) is used as an indicator for the degree of the defects in the graphene or the edges as well as the average size of crystalline sp^2 clusters (L_a) based on the well-known Tuinstra-Koenig relation $I_D/I_G = C(\lambda)/L_a$, where the proportionality constant $C(\lambda)$ depends on the excitation laser wavelength (λ).⁴⁹ Fig. 3a and b show the Raman spectra of different areas on the graphene membrane marked with letters in Fig. 1a. As can be seen in Fig. 3a, the low intensity of the D

peak of OGP1 is located at $\sim 1350\text{ cm}^{-1}$ which is consistent with few defects or may be caused by domain boundaries. The I_D/I_G of nONGP (~ 0.52) is higher than OGP1 (~ 0.35), which indicates more defects exist in nONGP (Fig. 3c). The shape of the 2D band and the ratio of its intensity relative to that of the G band (I_G/I_{2D}) are well-established characteristics of graphene layers.⁵⁰⁻⁵² As can be calculated from the Raman spectra in Fig. 3a and b, the ratios of G-band and 2D-band (I_G/I_{2D}) are 1.62 and 1.46, respectively, corresponding to the I_G/I_{2D} of multilayer graphene.^{16,21} The full width at half-maximum (FWHM) of the 2D peak for OGP1 was $85 \pm 5\text{ cm}^{-1}$, which is broader than trilayer graphene (74 cm^{-1}) reported before.⁵³ The stacking orders of graphene can also be observed from the differences in the line shape of the Raman 2D-mode.^{54,55} It can be seen more clearly in Fig. S3 that the 2D peak of OGP1 is fitted by a symmetric peak without shoulder, which is characteristic of high quality and well-ordered layer stacking graphene.⁵⁶ The similar shape, location and intensity of Raman peaks at random regions of OGP1 are consistent with the results of AFM characterization, which suggests OGP1 membrane is homogeneous and uniform as well. Compared to the I_G/I_{2D} of OGP1, the I_G/I_{2D} of OGP2 is much greater, which indicates that the OGP1 has fewer layers than the OGP2. Meanwhile, the larger I_D/I_G (~ 0.86) in Fig. 3d indicates more defects exist in OGP2 than OGP1, which suggests that the defect is also related to the layers of graphene prepared with present method.^{40,48} The defects of multilayer graphene with respect to those of reported graphene mainly derive from uneven distribution of heat during rapid cooling. As the thickness of the membrane increasing, the heat distribution is more uneven and thus results in more defects. Based on the Raman characterization, it can be concluded that the orientation behavior of PE has a great effect on the structure of graphene.

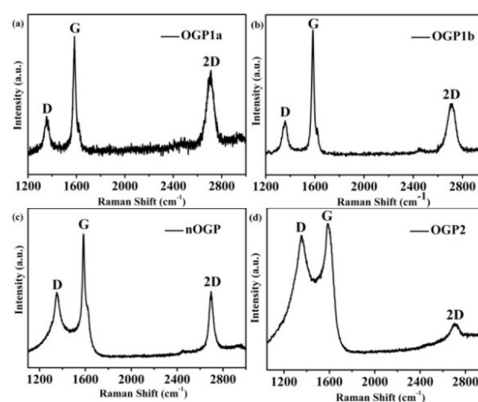


Fig. 3 Raman spectra of (a-b) different locations of OGP1 film corresponding to the letters "a" and "b" denoting in Fig. 1a, (c) nONGP and (d) OGP2.

Fig. 4a and b show typical scanning electron microscopic (SEM) images of OGP1 film on the copper crystal surface. It can be seen that the grown graphene covers the full copper surface. Moreover, the OGP1

film is continuous and homogeneous. Therefore, large area graphene film with dozens of microns can be obtained by this method. On the contrary, the nOGP film is inhomogeneous and contains lots of defects.

The typical surface morphologies of OGP1 and nOGP revealed by SEM after transferred onto Si substrates are also shown in Fig. 4c and d. SEM images (Fig. 4c) of OGP1 in high magnifications also manifest that a large area of uniform and continuous graphene film was obtained. Compared to OGP, the surface of nOGP is less homogeneous which can be seen from Fig. 4d. Meanwhile, the surface of OGP1 is relatively flat, which further confirms the results obtained by Raman spectroscopy. This is possibly caused by the different growth mechanism of graphene.

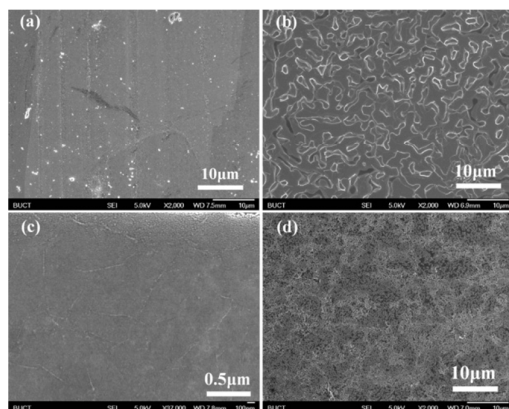


Fig. 4 SEM images of (a) OGP1 and (b) nOGP films grown on Cu substrate. The images shown in parts (c) and (d) display the OGP1 and nOGP films after transferring onto SiO₂/Si substrate.

In order to determine the orientation of the different sheets in the graphene film, the grown graphene was transferred onto the copper grid supported by amorphous carbon membrane or micro grid for transmission electron microscopic (TEM) observation. The transferred graphene showed minimal distortion or wrinkling on the copper grid with the amorphous carbon supporting membrane, as confirmed by low resolution TEM image shown in Fig. 5a. Higher resolution bright field images taken at the edges of the films shown in Fig. 5b and Fig. 5c directly prove that the OGP1 films are multilayered. The select-area electron diffraction (SAED) pattern (Fig. 5d) was acquired from the corresponding graphene film and showed one set of diffraction pattern characteristic of unique regular lattice stacking, other than at the grain boundaries. It reveals that the graphene sheets in film arrange in only one orientation. The nonuniform distribution of diffraction intensity also indicates that the graphene is composed of multiple layers with fine lattice matching.^{57, 58} Similar diffraction pattern could be detected at other randomly selected areas (Fig. S4b), suggesting a uniform ordered structure of obtained OGP1 multiple layers.^{41, 42, 59}

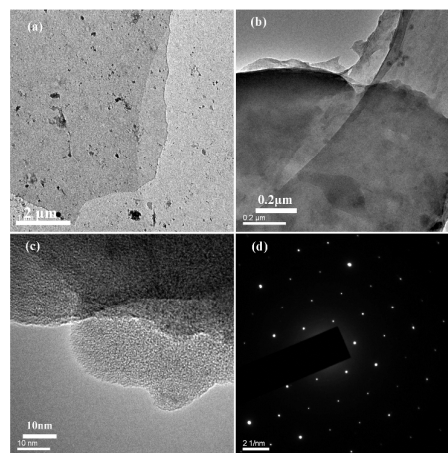


Fig. 5 TEM analysis of OGP1. (a) Low magnification TEM image of OGP1 sheet on the copper grid with an amorphous carbon support layer. (b) Bright field TEM image of OGP1 sheet on a micro grid. (c) High resolution TEM image at the edge of OGP1 film. (d) SAED pattern of OGP1.

OGP2 shows thicker edge than that of OGP1 in the high resolution bright field images as shown in Fig. 6a. SAED pattern of a continuous graphene film shown in Fig. 6a are presented in Fig. 6b. Compared to OGP1, the intensity of the diffraction spots of OGP2 becomes stronger. This change can attribute to the increasing graphene layers of OGP2. Likewise, similar distribution of diffraction pattern and intensity at the other random areas were detected (Fig. S4d). Thus, it is clear that the graphene sheets in film adopt the same orientation. We can draw a conclusion that the orientation and stacking order of graphene sheets is not affected by the number of layers. On the contrary, the SAED pattern of nOGP (Fig. 6d) shows several sets of diffraction pattern, which is different from the OGP. Measuring the angle between the selected adjacent diffraction points revealed a 20° rotation between the two sets of lattices, which indicates that nOGP is consisting of multiple layers with different layer orientations.^{40, 57, 60}

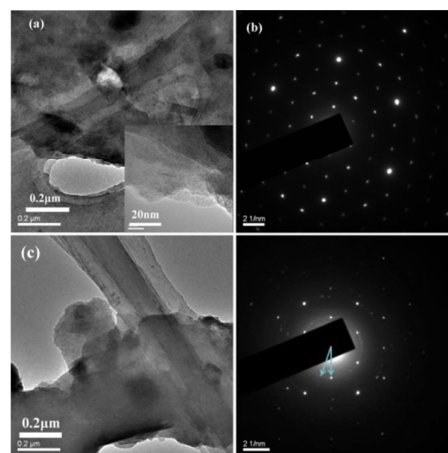


Fig. 6 TEM analysis of OGP2 and nOGP. (a) Bright field TEM image of OGP2 sheet on a micro grid; high resolution TEM image obtained at the edge of the film is shown in the insert. (b) SAED pattern of OGP2. (c) Bright field TEM image

of nOGP sheet on a micro grid. (d) SAED pattern of nOGP. The arrows show the rotation between the selected adjacent diffraction points.

Based on the characterization of SEM and TEM, it can be concluded that the OGP sheets grow layer by layer uniformly while the nOGP sheets grow randomly and unevenly. This is probably caused by the chain orientation of PE. For OPE, the molecular chains exhibit high orientation and arrange regularly and uniformly into the lamellae as shown in scheme 1. Therefore, lower energy may be needed in the growing process so that the graphene layers grow uniformly following the regular structure of PE lamellae in the direction perpendicular to the lamellae, which results in layer stacking with exact same orientation. As for nOPE, the molecular chains arrange randomly, which may require higher energy for initiating the formation of graphene. The formation of graphene may be explained as follows: the carbon chain in PE is rearranging in order to form hexatomic ring so that more energy is required for nOPE and it will result in less regular and uniform structure. Meanwhile, the formation of adjacent layers tends to achieve the minimum internal energy, resulting in lattice dislocation.^{41, 42} In general, the graphene sheets in OGP1 consist of well-ordered layer stacking which forms an ideal lattice matching. Unlike to OGP1, nOGP is composed of graphene sheets with lattice displacement.

As a high quality transparent conductive electrode, optical and electrical properties of graphene are vital. The optical and electrical properties of the continuous OGP1, OGP2 and nOGP graphene films formed on quartz were characterized by UV-vis spectroscopy and conductivity measurements. Fig. 7a shows the transmittance spectra of the graphene films, which have high transmittance in the visible and near-IR regions. At a wavelength of 550 nm, the transmittance of OGP1 was ~93.6%, and its sheet resistance was ~424 Ω /square at room temperature (Fig. 7a, b). By contrast, the transmittance of nOGP measured at the same condition decreased to ~91.6%, while its sheet resistance increased to ~1591 Ω /square (Fig. 7a, b). This change indicates that OGP1 has better optical and electrical performance than nOGP with similar thickness, which may be attributed to the well stacking structure of OGP1. The sheet resistance of OGP2 reached ~76 Ω /square, but the OGP2 film still had a transmittance of 88.2% at 550nm wavelength. It is worth mentioning that the transmittance of OGP1 and OGP2 was also much higher than the multilayer graphene obtained by many other methods with similar thickness, which can be attributed to the well-ordered stacking behaviour with unique lattice orientation. Moreover, the as-made OGP1 and OGP2 retain high electrical conductivity with only a slight increase in resistance at low and high temperatures. Comparing to OGP, the sheet resistance of nOGP increased significantly with increasing temperatures. This suggests that the OGP films contain less disordered

structures.⁶¹ The average resistance histogram for large numbers of devices showed that the room-temperature resistance of OGP1 was less than half of nOGP, and about 6 times higher than OGP2 (Fig. 7c). The sheet resistance of OGP is close to that of wet-transferred graphene⁶² with comparable transmittance, which is lower than those of reported graphene formed by CVD, oxygen-aided CVD,³⁹ chemically reduced method,^{63, 64} and Ni-catalyzed method.^{15, 16} Bae et al.⁶⁵ reported that graphene films had sheet resistances as low as ~125 Ω /square with 97.4% optical transmittance, suggesting that there is still room for improving the quality of OGP for use in transparent conducting electrode applications. Nevertheless, OGP is well structured, uniform and continuous with large area, and the current properties meet the requirements for practical applications in electrostatic dissipation, cathode ray tubes, and touch screens.⁶⁶

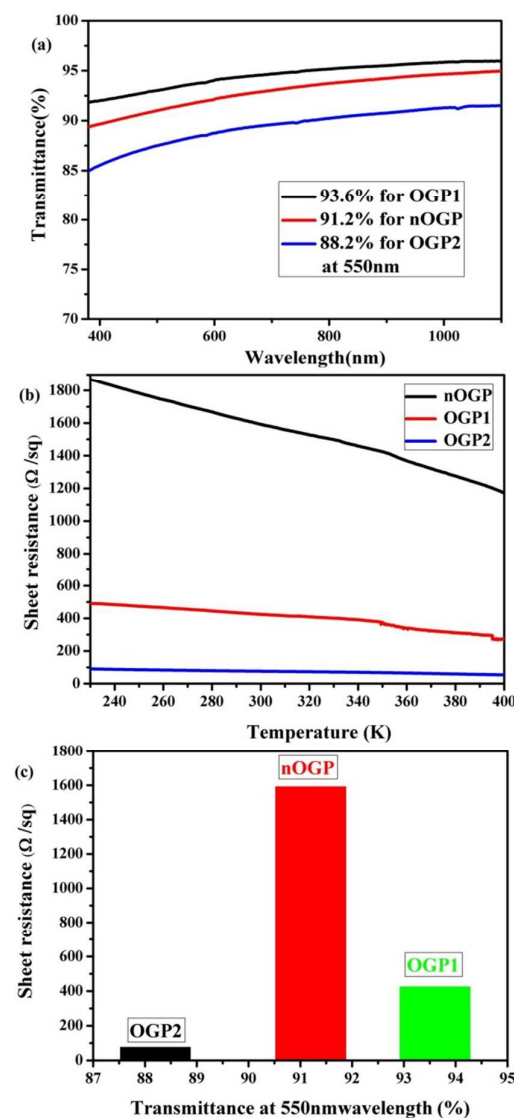


Fig. 7 Optical and electrical properties of OGP1, OGP2 and nOGP films on quartz. (a) Transmittance spectra of OGP1,

OGP2 and nOGP films on quartz. (b) Sheet resistance of OGP1, OGP2 and nOGP films in various temperature. (c) Mean resistance histograms for 10 devices based on OGP1, OGP2 and nOGP.

4. Conclusion

In summary, we have developed a new way for growing well-ordered multilayer graphene from OPE. The thickness of the graphene layer can be controlled. It is demonstrated that the lattice structure of the graphene layers plays a very important role in the optical and electrical characteristics. In contrast to OGP, nOGP show worse optical and electrical characteristic owing to its lattice displacement caused by the non-oriented structure of polymer precursor (nOPE). The optical and electrical measurements confirm that the performance of OGP is stable in air conditions and much higher than those reported. Thus, optimizing the structure of graphene based on our work may provide a new route toward preparation of graphene with controlled optical and electronic properties and find its unique applications for high quality transparent conductive electrode.

Acknowledgements

For financial support of this research, we thank the National Natural Science Foundation of China (91027043 and 21104002), 973 Program (Grant 2011CB932301, 2011CB605602 and 2012CB932903), NSFC-DFG Joint Project TRR61, the program of Introducing Talents of Discipline to Universities (B08003), Beijing Higher Education Young Elite Teacher Project (YETP0491) and the Chinese Academy of Sciences.

Notes and references

a State Key Laboratory of Chemical Resource Engineering, Beijing University of Chemical Technology, Beijing 100029, China. E-Mail: skyan@mail.buct.edu.cn. Tel: 010-64455928

b Beijing National Laboratory for Molecular Sciences, Institute of Chemistry, Chinese Academy of Sciences, Beijing 100190, China. E-Mail: wangzhaohui@iccas.ac.cn. Tel: 010-82616937

† Electronic Supplementary Information (ESI) available: [Supporting figures and characterization details]. See DOI: 10.1039/b000000x/

- K. S. Novoselov, A. K. Geim, S. V. Morozov, D. Jiang, Y. Zhang, S. V. Dubonos, I. V. Grigorieva and A. A. Firsov, *Science*, 2004, **306**, 666-669.
- S. J. Chae, F. Güneş, K. K. Kim, E. S. Kim, G. H. Han, S. M. Kim, H.-J. Shin, S.-M. Yoon, J.-Y. Choi, M. H. Park, C. W. Yang, D. Pribat and Y. H. Lee, *Adv. Mater.*, 2009, **21**, 2328-2333.
- X. Zhang, J. Ning, X. Li, B. Wang, L. Hao, M. Liang, M. Jin and L. Zhi, *Nanoscale*, 2013, **5**, 8363-8366.
- P. W. Sutter, J.-I. Flege and E. A. Sutter, *Nat. Mater.*, 2008, **7**, 406-411.
- C. Berger, Z. Song, X. Li, X. Wu, N. Brown, C. Naud, D. Mayou, T. Li, J. Hass and A. N. Marchenkov, *Science*, 2006, **312**, 1191-1196.
- T. Ohta, A. Bostwick, T. Seyller, K. Horn and E. Rotenberg, *Science*, 2006, **313**, 951-954.
- D. Li, M. B. Muller, S. Gilje, R. B. Kaner and G. G. Wallace, *Nat. Nanotechnol.*, 2008, **3**, 101-105.
- D. A. Dikin, S. Stankovich, E. J. Zimney, R. D. Piner, G. H. B. Dommett, G. Evmenenko, S. T. Nguyen and R. S. Ruoff, *Nature*, 2007, **448**, 457-460.
- S. Stankovich, D. A. Dikin, G. H. Dommett, K. M. Kohlhaas, E. J. Zimney, E. A. Stach, R. D. Piner, S. T. Nguyen and R. S. Ruoff, *Nature*, 2006, **442**, 282-286.
- Y. Xu, K. Sheng, C. Li and G. Shi, *J. Mater. Chem.*, 2011, **21**, 7376-7380.
- B. He, Y. Shen, Z. Ren, C. Xiao, W. Jiang, L. Liu, S. Yan, Z. Wang and Z. Yu, *Org. Electron.*, 2014.
- H. Bai, C. Li and G. Shi, *Adv. Mater.*, 2011, **23**, 1089-1115.
- H. Qian, F. Negri, C. Wang and Z. Wang, *J. Am. Chem. Soc.*, 2008, **130**, 17970-17976.
- J. Cai, P. Ruffieux, R. Jaafar, M. Bieri, T. Braun, S. Blankenburg, M. Muoth, A. P. Seitsonen, M. Saleh and X. Feng, *Nature*, 2010, **466**, 470-473.
- A. Reina, X. Jia, J. Ho, D. Nezich, H. Son, V. Bulovic, M. S. Dresselhaus and J. Kong, *Nano Lett.*, 2009, **9**, 30-35.
- K. S. Kim, Y. Zhao, H. Jang, S. Y. Lee, J. M. Kim, K. S. Kim, J. H. Ahn, P. Kim, J. Y. Choi and B. H. Hong, *Nature*, 2009, **457**, 706-710.
- X. Li, W. Cai, J. An, S. Kim, J. Nah, D. Yang, R. Piner, A. Velamakanni, I. Jung, E. Tutuc, S. K. Banerjee, L. Colombo and R. S. Ruoff, *Science*, 2009, **324**, 1312-1314.
- P. W. Zhancheng Li, Chenxi Wang, Xiaodong Fan, Wenhua Zhang, Xiaofang Zhai, Changgan Zeng, and J. Y. Zhenyu Li, Jianguo Hou, *ACS nano*, 2011, **5**, 3385-3390.
- J. Y. Zhong Jin, Carter Kittrell, James M. Tour, *ACS Nano*, 2011, **5**, 4112-4117.
- Y. Xue, B. Wu, L. Jiang, Y. Guo, L. Huang, J. Chen, J. Tan, D. Geng, B. Luo, W. Hu, G. Yu and Y. Liu, *J Am Chem Soc*, 2012, **134**, 11060-11063.
- Z. Sun, Z. Yan, J. Yao, E. Beitler, Y. Zhu and J. M. Tour, *Nature*, 2010, **468**, 549-552.
- B. L. J. Wei Liu, Jing Zhu, Cong-Qin Miao, Choon-Heui Chung, Young -Ju Park, Ke Sun, Jason Woo, Ya-Hong Xie, *ACS Nano*, 2010, **4**, 3927-3932.
- S. Pang, Y. Hernandez, X. Feng and K. Müllen, *Adv. Mater.*, 2011, **23**, 2779-2795.
- M. S. Kang, K. T. Kim, J. U. Lee and W. H. Jo, *J. Mater. Chem. C*, 2013, **1**, 1870-1875.
- Y. Liu, Q. Chang and L. Huang, *J. Mater. Chem. C*, 2013, **1**, 2970-2974.
- Y. Fang, B. Luo, Y. Jia, X. Li, B. Wang, Q. Song, F. Kang and L. Zhi, *Adv. Mater.*, 2012, **24**, 6348-6355.
- K. Zhang, L. L. Zhang, X. Zhao and J. Wu, *Chem. Mater.*, 2010, **22**, 1392-1401.
- Y. Wang, Z. Shi, Y. Huang, Y. Ma, C. Wang, M. Chen and Y. Chen, *J. Phys. Chem. C*, 2009, **113**, 13103-13107.
- K. Sheng, Y. Sun, C. Li, W. Yuan and G. Shi, *Scientific reports*, 2012, **2**.
- Y. Shao, H. Wang, Q. Zhang and Y. Li, *J. Mater. Chem. C*, 2013, **1**, 1245-1251.
- X. Wang, L. Zhi and K. Müllen, *Nano Lett.*, 2008, **8**, 323-327.
- B. Wang, X. Li, X. Zhang, B. Luo, M. Jin, M. Liang, S. A. Dayeh, S. Picraux and L. Zhi, *ACS nano*, 2013, **7**, 1437-1445.
- X. Wan, Y. Huang and Y. Chen, *Accounts. Chem. Res.*, 2012, **45**, 598-607.
- J. Wang, M. Liang, Y. Fang, T. Qiu, J. Zhang and L. Zhi, *Adv. Mater.*, 2012, **24**, 2874-2878.
- H. Bi, F. Huang, J. Liang, X. Xie and M. Jiang, *Adv. Mater.*, 2011, **23**, 3202-3206.
- S. Yan, I. Lieberwirth, F. Katzenberg and J. Petermann, *J. Macromol. Sci. B*, 2003, **42**, 641-652.
- J. Petermann and R. Gohil, *J. Mater. Sci.*, 1979, **14**, 2260-2264.

38. S. Yan and J. Petermann, *Polymer*, 2000, **41**, 6679-6681.
39. J. Chen, Y. Wen, Y. Guo, B. Wu, L. Huang, Y. Xue, D. Geng, D. Wang, G. Yu and Y. Liu, *J. Am. Chem. Soc.*, 2011, **133**, 17548-17551.
40. H. I. Rasool, E. B. Song, M. Mecklenburg, B. C. Regan, K. L. Wang, B. H. Weiller and J. K. Gimzewski, *J. Am. Chem. Soc.*, 2011, **133**, 12536-12543.
41. J. Hass, F. Varchon, J. Millán-Otoya, M. Sprinkle, N. Sharma, W. de Heer, C. Berger, P. First, L. Magaud and E. Conrad, *Phys. Rev. Lett.*, 2008, **100**.
42. S. Latil, V. Meunier and L. Henrard, *Phys. Rev. B*, 2007, **76**.
43. Z. P. Zheng Yan, Zhengzong Sun, Jun Yao, Yu Zhu, Zheng Liu, Pulickel M. Ajayan, James M. Tour, *ACS Nano*, 2011, **5**, 8187-8192.
44. B. Wu, D. Geng, Y. Guo, L. Huang, Y. Xue, J. Zheng, J. Chen, G. Yu, Y. Liu and L. Jiang, *Adv. Mater.*, 2011, **23**, 3522-3525.
45. J. W. Suk, W. H. Lee, J. Lee, H. Chou, R. D. Piner, Y. Hao, D. Akinwande and R. S. Ruoff, *Nano Lett.*, 2013, **13**, 1462-1467.
46. V. C. T. Matthew J. Allen, Richard B. Kaner, *Chem. Rev.*, 2010, **110**, 132-145.
47. L. M. Malard, M. A. Pimenta, G. Dresselhaus and M. S. Dresselhaus, *Phys. Rep.*, 2009, **473**, 51-87.
48. J. L. K. F. TUINSTRRA, *J. Chem. Phys.*, 1970, **53**, 1126-1130.
49. M. M. Lucchese, F. Stavale, E. H. M. Ferreira, C. Vilani, M. V. O. Moutinho, R. B. Capaz, C. A. Achete and A. Jorio, *Carbon*, 2010, **48**, 1592-1597.
50. D. Graf, F. Molitor, K. Ensslin, C. Stampfer, A. Jungen, C. Hierold and L. Wirtz, *Nano Lett.*, 2007, **7**, 238-242.
51. A. Gupta, G. Chen, P. Joshi, S. Tadigadapa and Eklund, *Nano Lett.*, 2006, **6**, 2667-2673.
52. Z. H. Ni, H. M. Wang, J. Kasim, H. M. Fan, T. Yu, Y. H. Wu, Y. P. Feng and Z. X. Shen, *Nano Lett.*, 2007, **7**, 2758-2763.
53. D. S. Lee, C. Riedl, B. Krauss, K. von Klitzing, U. Starke and J. H. Smet, *Nano Lett.*, 2008, **8**, 4320-4325.
54. M. S. Dresselhaus, A. Jorio, M. Hofmann, G. Dresselhaus and R. Saito, *Nano Lett.*, 2010, **10**, 751-758.
55. A. C. Ferrari, J. C. Meyer, V. Scardaci, C. Casiraghi, M. Lazzeri, F. Mauri, S. Piscanec, D. Jiang, K. S. Novoselov, S. Roth and A. K. Geim, *Phys. Rev. Lett.*, 2006, **97**.
56. C. H. Lui, Z. Li, Z. Chen, P. V. Klimov, L. E. Brus and T. F. Heinz, *Nano Lett.*, 2011, **11**, 164-169.
57. J. C. Meyer, A. K. Geim, M. I. Katsnelson, K. S. Novoselov, D. Obergfell, S. Roth, C. Girit and A. Zettl, *Solid State Commun.*, 2007, **143**, 101-109.
58. S. Horiuchi, T. Gotou, M. Fujiwara, R. Sotoaka, M. Hirata, K. Kimoto, T. Asaka, T. Yokosawa, Y. Matsui and K. Watanabe, *Jpn. J. Appl. Phys.*, 2003, **42**, L1073.
59. F. Varchon, P. Mallet, L. Magaud and J.-Y. Veuillen, *Phys. Rev. B*, 2008, **77**.
60. L. Gong, R. J. Young, I. A. Kinloch, S. J. Haigh, J. H. Warner, J. A. Hinks, Z. Xu, L. Li, F. Ding, I. Riaz, R. Jalil and K. S. Novoselov, *ACS Nano*, 2013, **7**, 7287-7294.
61. X. Li, G. Zhang, X. Bai, X. Sun, X. Wang, E. Wang and H. Dai, *Nat. Nanotechnol.*, 2008, **3**, 538-542.
62. X. Li, Y. Zhu, W. Cai, M. Borysiak, B. Han, D. Chen, R. D. Piner, L. Colombo and R. S. Ruoff, *Nano Lett.*, 2009, **9**, 4359-4363.
63. H. A. Becerril, J. Mao, Z. Liu, R. M. Stoltenberg, Z. Bao and Y. Chen, *ACS Nano*, 2008, **2**, 463-470.
64. H. Yamaguchi, G. Eda, C. Mattevi, H. Kim and M. Chhowalla, *ACS Nano*, 2010, **4**, 524-528.
65. S. Bae, H. Kim, Y. Lee, X. Xu, J.-S. Park, Y. Zheng, J. Balakrishnan, T. Lei, H. Ri Kim, Y. I. Song, Y.-J. Kim, K. S. Kim, B. Ozyilmaz, J.-H. Ahn, B. H. Hong and S. Iijima, *Nat. Nano*, 2010, **5**, 574-578.
66. M. Kaempgen, G. S. Duesberg and S. Roth, *Appl. Surf. Sci.*, 2005, **252**, 425-429.

Text:

We present here the synthesis and characterization of well Bernal (AB) stacked multilayer graphene from highly oriented polyethylene film. The obtained graphene films exhibit high optical and electrical properties.

